



# Comparative study of uncoated and tetraethylorthosilicate-coated magnetic chitosan beads in the adsorption of two textile dyes

F. Santillán<sup>1</sup> · I. M. M. Mejía<sup>1</sup> · H. C. Goicoechea<sup>2</sup>

Received: 1 February 2022 / Revised: 22 September 2022 / Accepted: 7 January 2023 / Published online: 17 January 2023

© The Author(s) under exclusive licence to Iranian Society of Environmentalists (IRSEN) and Science and Research Branch, Islamic Azad University 2023

## Abstract

Textile dyes are harmful to human health and aquatic ecosystems. To tackle this issue, an environmentally friendly alternative should be addressed. In this research, magnetic chitosan beads, uncoated (MCB) and coated (CMCB) with tetraethylorthosilicate (TEOS), were fabricated. The beads were synthesized using magnetite and TEOS-coated magnetite as starting materials and glutaraldehyde as a crosslinker through an ionotropic gelation method that includes the dropwise addition of a ferrofluid into a basic solution. The magnetic beads were characterized by several techniques, such as FT-IR, VSM, XRD, and SEM–EDX. In addition, the beads loaded with the adsorbed dye were also characterized to assess the stability of the materials after the adsorption process. MCB and CMCB were evaluated as adsorbents for textile dyes Synozol Red HF-6BN (SR) and Synozol Yellow HF-2GR (SY). For both dyes, the maximum removal efficiencies were obtained at pH 2 with 20 mg of adsorbent and 180 r min<sup>-1</sup>. Adsorption of both dyes followed the Freundlich model, and the maximum adsorption capacities were SR dye: 88.12 (MCB) and 192.02 (CMCB) mg g<sup>-1</sup>, SY dye: (MCB) and 70.5 (CMCB) mg g<sup>-1</sup>. The adsorption kinetics fitted well with the pseudo-second-order kinetic model. Reusability of the materials was also demonstrated. The modeling of the data gathered by the Box–Behnken design experiments helped corroborate the obtained experimental data and find the optimal pH, dye concentration, and adsorbent dose for dyes removal.

**Keywords** Magnetic beads · Removal · Synozol Red HF-6BN · Synozol Yellow HF-2GR

## Introduction

Many industries, such as textile, paper, and food processing, produce massive colored effluents (Haddad et al. 2018) that adversely affect species photosynthesis and human health (Samchetsabam et al. 2017; Lellis et al. 2019). The textile industry distinguishes itself owing to the high amounts of water in all its involved production stages (dyeing, finishing, and washing), leading to the generation of large volumes of

colored wastewater (de Assis Filho et al. 2021). Textile dyes are organic compounds that stain surfaces or fibers through various adhesion mechanisms, such as physical adsorption, mechanical retention, covalent bonds, and complexes with salts or metals. Over 50% of textile dyes are azoic (azo dyes), and some are reported as carcinogenic and release aromatic amines that damage aquatic ecosystems or epidermal cells (Benkhaya et al. 2020). The two azo dyes in this study are widely applied for dyeing cotton, silk, and synthetic polyester fibers. Synozol Red HF-6BN (SR) and Synozol Yellow HF-2GR (SY) are monoazo dyes that contain six and five sulfonic groups, respectively. The higher hydrophilicity of these dyes makes removal from effluents complex (Patil and Shukla 2015; Revathi et al. 2019; Singh et al. 2022).

Conventional methods for textile wastewater treatment include ozonation, flocculation, electrochemical oxidation, anaerobic remediation, bacterial decoloration, membrane filtration, and irradiation (Tabar and Toosi 2018; Dixit and Garg 2019; Xia et al. 2020; Wang et al. 2020; Adar 2020). However, most of these techniques have yet to achieve an effective removal and could generate harmful by-products. Over the last

Editorial responsibility: Chongqing Wang.

✉ I. M. M. Mejía  
imaza@uni.edu.pe

<sup>1</sup> Laboratorio de Investigación de Química Analítica y Ambiental, Universidad Nacional de Ingeniería, Av. Tupac Amaru 210, P.O. Box 15000, Rímac, Peru

<sup>2</sup> Laboratorio de Desarrollo Analítico y Quimiometría (LADAQ), Cátedra de Química Analítica I, Facultad de Bioquímica y Ciencias Biológicas, Universidad Nacional del Litoral, Ciudad Universitaria, S3000ZAA Santa Fe, Argentina



few years, adsorption has emerged as an attractive alternative owing to its effectiveness (Mustafa et al. 2020; Santillán and Rueda 2020), economic viability, and use of low-cost materials such as clays, activated carbon, agro-industrial waste, chitin, alginate, and chitosan.

Magnetic chitosan composites have attracted increased interest in wastewater treatment because of their ease of synthesis and the possibility of separating the pollutants from the adsorbents showing potential for reusability (Roh et al. 2019; Ayub et al. 2020). These adsorbents, consisting mainly of a chitosan matrix mixed with a dispersed phase of magnetic particles (magnetite or maghemite), have shown promising results in removing dyes and heavy metals (Mahdavinia et al. 2015; Moradlou et al. 2016; Kamari and Shahbazi 2021). To improve the efficiency of these composites and protect the magnetic core from degradation, modifications with silica-based materials, including 3-aminopropyltriethoxysilane (APTES), 3-mercaptopropyltrimethoxysilane (MPS), and tetraethylorthosilicate (TEOS), have been performed (Yang et al. 2016; Nnadozie and Ajibade 2020).

Recent reports (Danahoglu et al. 2018; Tian et al. 2022) have shown the successful removal of contaminants such as polychlorinated biphenyls and antibiotics from water samples using chitosan-grafted  $\text{SiO}_2\text{-Fe}_3\text{O}_4$  nanoparticles. However, the application of magnetic chitosan beads for SR and SY removal has not been studied exhaustively. To this end, the present study compared the performance of the magnetic composites uncoated and coated with TEOS.

Response surface methodology (RSM) is a helpful technique that allows researchers to develop, improve, or optimize a broad range of processes. This approach may work even when complete knowledge of the state and behavior of the subject system is lacking (Myers et al. 2009). Box–Benkhen stands out as well suited for RSM among the surface response designs. Based on this sense, a modified Box–Benkhen experimental design is performed to optimize some variables (pH, concentration, adsorbent dose) associated with the textile dyes adsorption process.

In this research, magnetic chitosan beads uncoated (MCB) and coated (CMCB) with TEOS were successfully prepared and evaluated for the removal of Synozol Red HF-6BN (SR) and Synozol Yellow HF-2GR (SY) dyes. The effect of pH, adsorbent dose, initial concentration, and shaking speed were studied. Adsorption equilibrium data and kinetics were also investigated. The research was conducted from April 2016 to April 2017 at "Universidad Nacional de Ingeniería", Lima, Peru.

## Material and methods

### Materials

Ferrous sulphate heptahydrate ( $\text{FeSO}_4 \cdot 7\text{H}_2\text{O}$ ), sodium hydroxide (NaOH), and potassium hydroxide (KOH) were purchased from Fermont. Tetraethylorthosilicate (TEOS), potassium nitrate, chitosan (196 kDa, degree of deacetylation 86.0%), glutaraldehyde, textile dyes, and solvents were all from Sigma-Aldrich USA. All the solutions were prepared with ultrapure water, which was obtained from a Thermo Fischer Scientific System.

### Synthesis of magnetite ( $\text{Fe}_3\text{O}_4$ ) and coated magnetite (C- $\text{Fe}_3\text{O}_4$ )

Colloidal magnetite particles ( $\text{Fe}_3\text{O}_4$ ) and TEOS-stabilized magnetite particles (C- $\text{Fe}_3\text{O}_4$ ) were prepared as described by our previous study (Muedas-Taípe et al. 2020).

### Preparation of magnetic chitosan beads (MCB) and coated magnetic chitosan beads (CMCB)

The synthesis of both magnetic beads has been described in our previous research (Muedas-Taípe et al. 2020). Briefly, 1.3 g of starting material (magnetite or coated magnetite) was dispersed into a 2% chitosan solution under sonication for 30 min. The obtained ferrofluid was added dropwise to a 2 M NaOH solution, leading to the formation of the beads. The beads were washed with deionized water and crosslinked with glutaraldehyde.

### Adsorption experiments

All adsorption experiments were carried out as batch type at 25 °C and by immersing beads in 10 mL of dye solution ( $50 \text{ mg L}^{-1}$ ) for 12 h and at  $180 \text{ r min}^{-1}$ . The parameters influencing the adsorption process were evaluated: initial pH, initial dye concentration adsorbent dose, and shaking speed.

Concentrations of SR and SY were quantified with a UV–Vis spectrophotometer at wavelengths of 501.5 nm and 407 nm, respectively. This calculation was applied to all the solutions before and after the adsorption process.

All experiments were performed in triplicate, and the amount of dye adsorbed ( $Q$ ) was calculated by the following equation (Eq. 1):

$$Q = \frac{(C_0 - C)V}{m} \quad (1)$$

where  $C_0$  and  $C$  ( $\text{mg L}^{-1}$ ) are the initial and final dye concentrations, respectively;  $V$  (L) is the volume of dye used; and  $m$  (g) is the mass of dried adsorbent.

The adsorption processes of both dyes were examined with Langmuir and Freundlich isotherm models (Freundlich 1906; Langmuir 1918). The linear equations (Eqs. 2, 3) of both models are given below, where  $C_e$  is the dye concentration at equilibrium ( $\text{mg L}^{-1}$ ),  $Q_e$  is the adsorption capacity of the adsorbent ( $\text{mg g}^{-1}$ ),  $Q_m$  is the maximum adsorption capacity of the adsorbent ( $\text{mg g}^{-1}$ ) and  $K_L$  is the adsorption equilibrium constant ( $\text{L mg}^{-1}$ ),  $K_F$  is the Freundlich constant ( $\text{L g}^{-1}$ ), and  $1/n$  is a parameter associated with adsorption intensity:

$$\frac{C_e}{Q_e} = \frac{1}{K_L Q_m} + \frac{C_e}{Q_m} \quad (2)$$

$$\log Q_e = \log K_F + \frac{1}{n} \log C_e \quad (3)$$

To investigate the effect of contact time on SR and SY removal for kinetic studies, 300 mL of dye solution ( $50 \text{ mg L}^{-1}$ , pH 2) was reacted with 600 mg of beads under different intervals of time.

Pseudo-first-order (Lagergren 1898) and pseudo-second-order (Ho and McKay 1998) kinetics were used to simulate the adsorption kinetics. Equations (Eqs. 4, 5) of both models can be expressed as:

$$\log (Q_e - Q_t) = \log Q_e - \frac{k_1 t}{2.303} \quad (4)$$

$$\frac{t}{Q_t} = \frac{1}{k_2 Q_e^2} + \frac{t}{Q_e} \quad (5)$$

where  $Q_t$  ( $\text{mg g}^{-1}$ ) and  $Q_e$  ( $\text{mg g}^{-1}$ ) are the amount of dye adsorbed at time  $t$  and under equilibrium conditions, respectively;  $k_1$  and  $k_2$  are the rate Lagergren and Ho constants for adsorption, respectively.

### Desorption and reusability experiments

Before desorption experiments, the magnetic composites (loaded with dye) were isolated using a magnetic field. Then, the dye-loaded beads were immersed into a 2 M NaOH solution at  $25^\circ\text{C}$  for 30 min and separated with a magnet. The desorbed beads were dried at room temperature to repeat some adsorption experiments.

The reusability of the magnetic chitosan beads (MCB and CMCB) was evaluated by immersing 20 mg of the desorbed beads into a  $50 \text{ mg L}^{-1}$  dye solution (pH 2) and letting it react between 2 and 3 h at  $180 \text{ r min}^{-1}$ . After the adsorption, the efficiency of the beads was calculated.

### Structural characterization

Starting materials and beads were structurally characterized by Fourier Transformed Infrared Spectroscopy (FTIR, ATR mode, IR-Prestige 21 Shimadzu) in the range of  $4000\text{--}400 \text{ cm}^{-1}$ , with a resolution of  $4 \text{ cm}^{-1}$  and 32 scans. Raman spectra were acquired with a XploRA—Horiba Scientific spectrometer with a 532 or 785 nm laser. Surface morphology and elemental composition of the samples were determined by scanning electron microscopy with X-ray dispersive energy (SEM–EDX, Carl Zeiss EVO MA 10). X-Ray diffraction (XRD) measurements were performed on a D5000 DIFFRAC PLUS Siemens diffractometer.

The magnetic properties of the samples at room temperature were studied using a vibration sample magnetometer (built for research in the Laboratory of Nanostructured Materials of the National University of Engineering, Peru).

### Experimental design

Experimental design was performed to find the optimal conditions for removing azo dyes from the synthetic samples. To this end, two slightly modified Box–Behnken designs were built for each type of bead to carry out the experiments. With the two designs, it could check out the effect of three fundamental variables in dye removal (pH, dye concentration, and adsorbent dose).

RSM is based on building a mathematical model for each response by fitting a second-order polynomial expression of the response as a function of the factors. The general form of the second-order expression can be written as follows (Eq. 6):

$$y = \beta_0 + \sum_{i=1}^k \beta_i x_i + \sum_{i=1}^k \beta_{ii} x_i^2 + \sum_{1 \leq i < j}^k \beta_{ij} x_i x_j + \varepsilon \quad (6)$$

where  $y$  represents the response,  $x_i$  and  $x_j$  are the factors,  $\beta_0$  is the constant term or intercept,  $\beta_i$ ,  $\beta_{ii}$ , and  $\beta_{ij}$  are the coefficients of linear, quadratic, and interacting terms, respectively, and  $\varepsilon$  is a residual term. Usually, only two-factor interactions are considered (Myers et al. 2009).

Several types of designs can be used to implement RSM. In particular, the Box–Behnken design can be used in optimization, effectively optimizing a process involving several parameters simultaneously with a reduced number of experiments (Vera Candiotti et al. 2014).

In addition, the so-called Derringer's desirability function becomes a powerful tool when different responses have to be optimized simultaneously (Derringer and Suich 1980). For its application, a partial desirability function ( $d_i$ ) must be created for each individual response using the fitted models. This step requires an optimization criterion to select the most desirable ranges for each design factor or response:



maximization, minimization, maintaining a range, or reaching a target value. Besides, a weight ( $w_i$ ) can be given to each goal. After that, the global desirability function ( $D$ ) can be computed using the following equation (Eq. 7):

$$D = (d_1^{r_1} \times d_2^{r_2} \times \dots \times d_n^{r_n})^{\frac{1}{\sum r_i}} = \left( \prod_{i=1}^n d_1^{r_i} \right)^{\frac{1}{\sum r_i}} \quad (7)$$

where  $n$  is the number of variables included in the optimization procedure and  $r_n$  is the importance of each factor or response relative to the others.

## Software

Experimental design, surface response modeling, and desirability function calculations were performed using the StatEaseDesign–Expert 8.0.0 (Stat–Ease, Inc, Minneapolis, USA).

## Results and discussion

### Structural characterization of the synthesized materials

#### Fourier transformer infrared spectroscopy

FT-IR analysis was performed to determine the presence of functional groups in the starting materials and magnetic composites (beads).

Figure S2a shows the spectra of synthesized magnetite ( $\text{Fe}_3\text{O}_4$ ) and coated magnetite ( $\text{C-Fe}_3\text{O}_4$ ). For both materials, it is noticed the peak corresponds to  $\delta(\text{Fe-O})$  torsional vibration when the iron is in octahedral sites at  $427 \text{ cm}^{-1}$  and  $480 \text{ cm}^{-1}$  for  $\text{Fe}_3\text{O}_4$  and  $\text{C-Fe}_3\text{O}_4$ , respectively (Radoń et al. 2020). The strong peak at  $576 \text{ cm}^{-1}$ , assigned to  $\nu(\text{Fe-O})$  stretching vibration when the Fe is in tetrahedral sites, also appears in the spectrum of  $\text{Fe}_3\text{O}_4$ . Furthermore, for  $\text{C-Fe}_3\text{O}_4$ , the following peaks could be observed:  $800 \text{ cm}^{-1}$  (Si–O–Fe bond),  $954 \text{ cm}^{-1}$  (Si–O symmetric stretching), and  $1080 \text{ cm}^{-1}$  (asymmetric Si–O–Si bond). These results are consistent with the literature (de Mendonça et al. 2019; Dayana et al. 2019), indicating the effective coating of magnetite. Figure S2b shows the infrared spectra of the adsorbents (MCB and CMCB), in which some peaks of chitosan can be observed (Fig. S1, Table S1). Both spectra display a similar shape; however, the strong and sharp peak at  $1024 \text{ cm}^{-1}$  indicates the presence of the Si–O–Si bond in CMCB. The latter enabled corroborating an effective synthesis of coated magnetic chitosan beads (Yue et al. 2018).

Beads after an adsorption process were also characterized by FT-IR. Figure S2c depicts the spectra of SR, SR–MCB,

and SR–CMCB, and Fig. S2d shows the spectra of SY, SY–MCB, and SY–CMCB.

For both azo dyes, the following main bands were determined: stretching vibrations of –NH and –OH groups at  $3452$  (SR) and  $3450 \text{ cm}^{-1}$  (SY), asymmetric stretching of the aliphatic –CH at  $2921$  and  $2848 \text{ cm}^{-1}$  (SY), vibration of aromatic rings at  $1620 \text{ cm}^{-1}$  (SR), stretching of the azo group –N=N– at  $1545$  (SR) and  $1553 \text{ cm}^{-1}$  (SY), vibrational stretching of the C–N at  $1489$  (SY),  $1397$  (SY) and  $1389 \text{ cm}^{-1}$  (SR), vibration of S=O ( $\text{SO}_2$ ) at  $1322 \text{ cm}^{-1}$ , vibration of S=O ( $\text{SO}_3^-$ , sulfonic groups) at  $1128$  (SR) and  $1131 \text{ cm}^{-1}$  (SY), stretching of –C–OH and/or –CN at  $1039 \text{ cm}^{-1}$  (SY, SR), vibrational stretching of –S=O at  $670$  (SR) and  $671 \text{ cm}^{-1}$  (SY). These obtained bands match with the reported spectra (Patil and Shukla 2015; Pérez-Calderón et al. 2018).

FT-IR spectra of beads with adsorbed SR (SR–MCB, SR–CMCB) showed a decrease in the intensity of all peaks. There is a pronounced reduction in the vibration of S=O ( $\text{SO}_3^-$ ) in the spectrum of SR–CMCB compared to the magnetic chitosan beads, which indicates a strong interaction between the SR dye and coated magnetic chitosan beads because TEOS coating increases the number of negative charges on the surface of the adsorbent. Furthermore, this could support the occurrence of electrostatic interaction between protonated amino groups of chitosan ( $\text{NH}_3^+$ ) and sulfonic groups ( $\text{SO}_3^-$ ) of the dye (Pérez-Calderón et al. 2020). A similar trend was observed for the adsorbents after the adsorption of SY.

#### Raman spectroscopy

Raman spectroscopy allows the determination of some functional groups that cannot be detected by infrared spectroscopy. In this context, this technique helped to characterize the synthesized starting materials, and the characteristic peaks are indicated in Table 1.

Figure S3 depicts the Raman results of magnetite ( $\text{Fe}_3\text{O}_4$ ) and TEOS-coated magnetite ( $\text{C-Fe}_3\text{O}_4$ ). Both spectra showed a very similar shape, but  $\text{C-Fe}_3\text{O}_4$  highlights the presence of the Si–O–Si bond at  $900 \text{ cm}^{-1}$  and  $\text{SiO}_2$  at  $482 \text{ cm}^{-1}$ .

**Table 1** Functional groups corresponding to Raman spectrum of synthesized  $\text{Fe}_3\text{O}_4$  and  $\text{C-Fe}_3\text{O}_4$

Functional group	$\text{cm}^{-1}$
Fe–O ( $T_{2g}$ )	219 ( $\text{Fe}_3\text{O}_4$ ), 211 ( $\text{C-Fe}_3\text{O}_4$ )
Fe–O ( $T_{2g}$ )	280 ( $\text{Fe}_3\text{O}_4$ ), 281 ( $\text{C-Fe}_3\text{O}_4$ )
$\text{OH}^-$ from $\text{Fe}_3\text{O}_4$ surface	395 ( $\text{Fe}_3\text{O}_4$ ), 386 ( $\text{C-Fe}_3\text{O}_4$ )
Presence of $\text{SiO}_2$	482 ( $\text{C-Fe}_3\text{O}_4$ )
Si–O–Si	900 ( $\text{C-Fe}_3\text{O}_4$ )
Magnon	1310 ( $\text{Fe}_3\text{O}_4$ ), 1309 ( $\text{C-Fe}_3\text{O}_4$ )

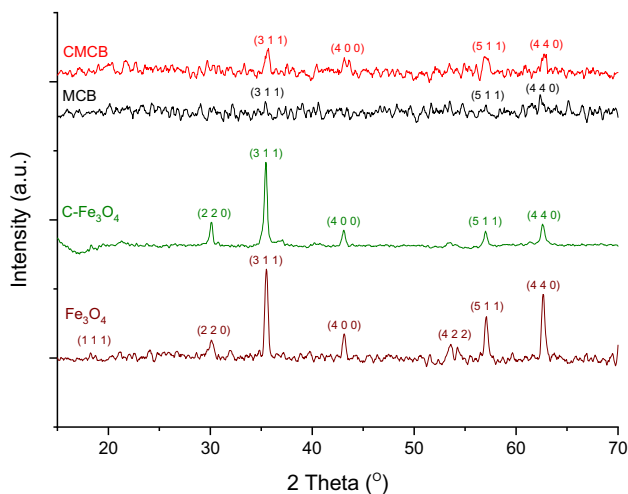




Moreover, the intensity of the strong peak at  $1310\text{ cm}^{-1}$  ( $\text{Fe}_3\text{O}_4$ ) associated with a magnon decreases in the spectrum of C- $\text{Fe}_3\text{O}_4$  ( $1309\text{ cm}^{-1}$ ). These features strongly supported a good coating of the magnetite's surface with TEOS.

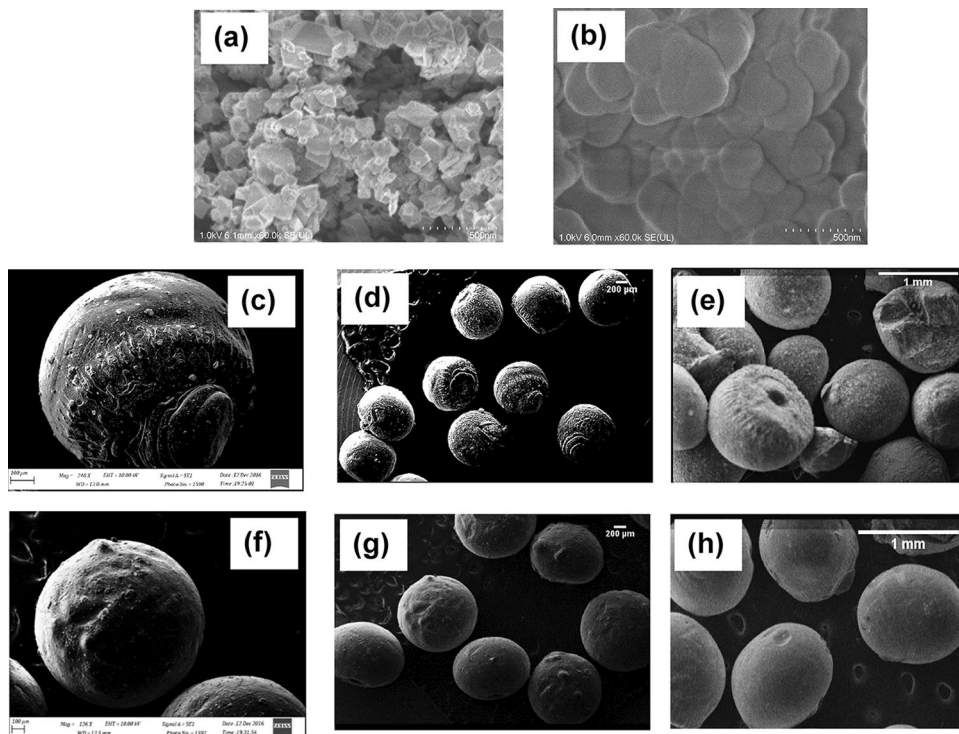
### X-Ray diffraction

Figure 1 shows the XRD patterns of magnetite, coated magnetite, MCB, and CMCB. These measurements were carried out in a range from  $10^\circ$  to  $70^\circ$ .



**Fig. 1** XRD patterns of  $\text{Fe}_3\text{O}_4$ , C- $\text{Fe}_3\text{O}_4$ , MCB, and CMCB

**Fig. 2** SEM images of **a**  $\text{Fe}_3\text{O}_4$ , **b** C- $\text{Fe}_3\text{O}_4$ , **c**, **d** MCB, **e** MCB after SR adsorption, **f**, **g** CMCB, **h** CMCB after SR adsorption



The synthesized magnetite presents the following characteristics peaks (1 1 1) (2 2 0) (3 1 1) (4 0 0) (4 2 2) (4 4 0) (5 1 1) that are consistent with the crystalline structure of magnetite previously reported (de Mendonça et al. 2019; Radoń et al. 2020). On the other hand, C- $\text{Fe}_3\text{O}_4$  showed the same diffraction peaks with lower intensity, indicating that the stabilization with TEOS did not significantly influence the crystalline structure. Besides, since TEOS is an amorphous material, it could cause a reduction in intensity.

The crystal structure of beads was also investigated. MCB and CMCB still showed the presence of peaks associated with the magnetite XRD pattern. However, the crystallinity of both types of beads is affected by the presence of chitosan, which according to previous reports is amorphous (Zhang et al. 2020).

A comprehensive comparison of MCB and CMCB diffractograms shows that CMCB crystallinity is slightly less affected than MCB. This characteristic strongly supports that coating with TEOS has no pronounced effect on a sample's crystallinity.

### Scanning electron microscopy and X-ray dispersive energy

SEM-EDX analysis allowed the study of the morphology of the materials and the determination of their respective chemical composition. SEM images of  $\text{Fe}_3\text{O}_4$  and C- $\text{Fe}_3\text{O}_4$  are shown in Fig. 2. Figure 2a shows the presence of mono-disperse microcrystals. In contrast, Fig. 2b shows a more

homogeneous surface, indicating that TEOS acts as a stabilizing agent and prevents the particles from agglomerations.

SEM images of MCB and CMCB demonstrate the spherical shape of the adsorbents (Fig. 2c–g) and highlight an improvement in the homogeneity of the surface in CMCB because of the coating with TEOS.

The beads were also characterized after a removal process. Due to the similarity of SR and SY structures, we chose one of the dye-adsorbed materials (beads with SR). Figure 2e, h shows SEM images of MCB and CMCB, respectively, and both with SR after the removal. For both cases, the morphology did not present significant variations; however, the MCB seems slightly destroyed.

EDX analysis of all the mentioned materials is presented in Table 2. For  $\text{Fe}_3\text{O}_4$  and  $\text{C-Fe}_3\text{O}_4$ , this technique indicates the presence of Fe, O, and C as their main components, and a significant content of Si (%) corroborates the desired coating for  $\text{C-Fe}_3\text{O}_4$ . For MCB and CMCB, the presence of Fe, O, N, and C is highlighted with the difference in the content of Fe and the increase in Si content (%). The latter helped

to corroborate the coating of beads with TEOS. As in our previous article (Muedas-Taipe et al. 2020), the high content of O compared to C (%) may suggest the coating of  $\text{Fe}_3\text{O}_4$  by some Si–O–Si bonds through a three-dimensional net.

Overall, for the beads after SR adsorption, the content of the elements decreased. The S (%) content could be associated with the dye's sulfonic groups ( $\text{SO}_3^-$ ) presence. MCB–SR showed higher S content than CMCB–SR, which may indicate a strong interaction between CMCB and the dye.

### Vibration sample magnetometry

Magnetization curves of  $\text{Fe}_3\text{O}_4$ ,  $\text{C-Fe}_3\text{O}_4$ , both types of beads, and CMCB–dye are shown in Fig. 3. The shape of all obtained curves displayed a complete hysteresis cycle, which indicates that all of them possess a ferrimagnetic behavior (Svetlichnyi et al. 2017).

The values of saturation magnetization ( $M_s$ ) of all materials were determined by the analysis of the obtained curves.

**Table 2** Elemental composition obtained by EDX for  $\text{Fe}_3\text{O}_4$ ,  $\text{C-Fe}_3\text{O}_4$ , MCB, CMCB, MCB–SR, CMCB–SR

Element	$\text{Fe}_3\text{O}_4$ (Wt%) <sup>c</sup>	$\text{C-Fe}_3\text{O}_4$ (Wt%)	MCB (Wt%)	CMCB (Wt%)	MCB–SR <sup>a</sup> (Wt%)	CMCB–SR <sup>b</sup> (Wt%)
Fe	51.56	14.32	20.85	6.0	26.0	0.2
O	39.18	68.2	37.19	35.98	20.4	29.1
Si	0	43.32	0	5.97	0	0.2
N	0	0	4.19	4.8	0	0
C	8.87	10.52	37.77	46.64	41.2	64.5
S	0	0	0	0	3.3	0.8

<sup>a</sup>Magnetic chitosan beads after SR adsorption

<sup>b</sup>Magnetic chitosan beads coated with TEOS after SR adsorption

<sup>c</sup>Weight percent

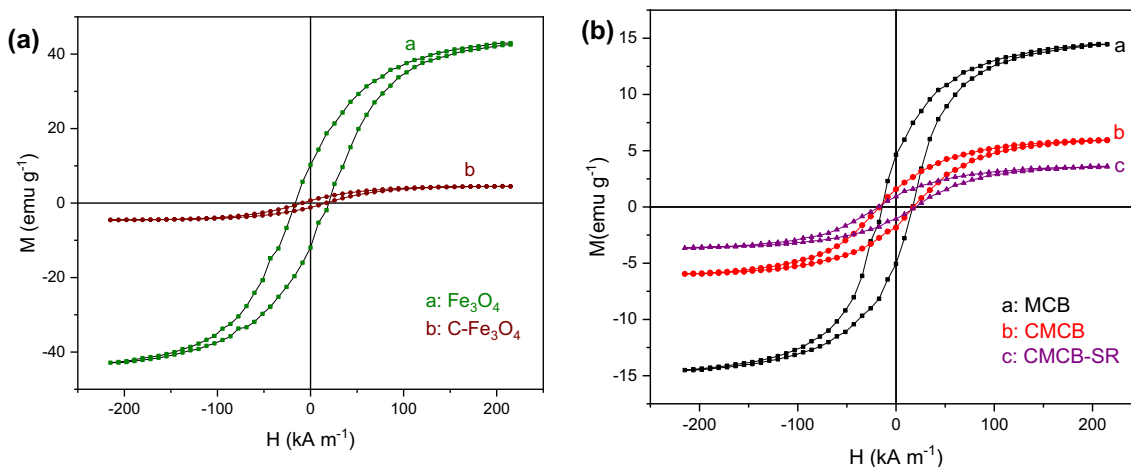


**Fig. 3** Magnetization curves of **a**  $\text{Fe}_3\text{O}_4$  and  $\text{C-Fe}_3\text{O}_4$ , **b** MCB, CMCB, and CMCB after SR adsorption

$M_s$  values of  $\text{Fe}_3\text{O}_4$  and  $\text{C-Fe}_3\text{O}_4$  were 43.6 and 4.18  $\text{emu g}^{-1}$ , respectively. This strong decrease may be produced by the coating with TEOS that reduces the magnetism of the adsorbent (de Mendonça et al. 2019).

Figure 3b shows that the  $M_s$  values for MCB, CMCB, and CMCB-dye were 14.3, 5.92, and 3.60  $\text{emu g}^{-1}$ , respectively. This trend may be explained because magnetite possesses more magnetic domains. For all of them to be aligned, it is necessary to have a high magnetization value compared to the other materials. The coating decreases the number of magnetic domains, and therefore, less magnetization is required.

Moreover, remnant magnetization ( $M_r$ ) values for MCB, CMCB, and CMCB-dye were 4.43 and 1.55  $\text{emu g}^{-1}$ , respectively. Those values confirm the applicability of the materials in processes where magnetic field separation is involved (Liu et al. 2012). CMCB after SR adsorption (CMCB-SR) was also characterized.  $M_s$  and  $M_r$  obtained values were 3.60 and 0.95  $\text{emu g}^{-1}$ , respectively. This would indicate the possibility of applying the material in one more cycle of the adsorption process.

## Adsorption experiments

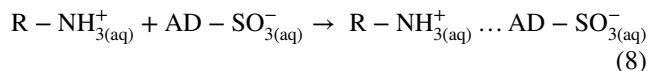
### Effect of pH

The initial pH of the solution is an important factor in the adsorption processes because it could affect the surface charge of the materials likewise their degree of ionization (Silva et al. 2020).

Figure 4 illustrates the effect of pH on SR and SY adsorption by MCB and CMCB. The selected range of pH values includes extreme acidic (pH 2) and basic conditions (pH 11). The experiments were carried out for 12 h with initial dye

concentrations of 50  $\text{mg L}^{-1}$ , a shaking speed of 180  $\text{r min}^{-1}$ , and a temperature of 25 °C.

According to this figure, under acidic conditions, there is a greater removal of the dyes than under basic conditions, with the maximum percentages of removal standing out at pH 2. This behavior is consistent with the proposed mechanism of dye sorption by chitosan (Pérez-Calderón et al. 2020) because its amino groups are protonated in an acidic medium. As a result, an electrostatic interaction occurs between these groups and sulfonic groups of the azo dyes (AD) SR and SY. The mechanism mentioned above can be depicted by the following equation (Eq. 8):



The effectiveness of the adsorbents decreases as the pH increases because there are fewer protonated amino groups. Comparing the percentage values of SR removal obtained with both adsorbents, there is an evident increase in the calculated values for CMCB (Table S2). As mentioned above, TEOS protects magnetite and makes it more resistant to extreme conditions such as pH 2. Similar results were obtained for the removal of SY.

Overall, the results of this test enhance carrying out the rest of the experiments using solutions at pH 2.

### Effect of adsorbent dose

The adsorbent dose is another crucial factor in the adsorption process that should be studied. The effect of adsorbent dose in SR and SY adsorption by MCB and CMCB is shown in Figs. 5, 6. This series of experiments was carried out using 10–80 mg of beads at pH 2, a temperature of 25 °C, a dye concentration of 50  $\text{mg L}^{-1}$ , and 180  $\text{r min}^{-1}$ .

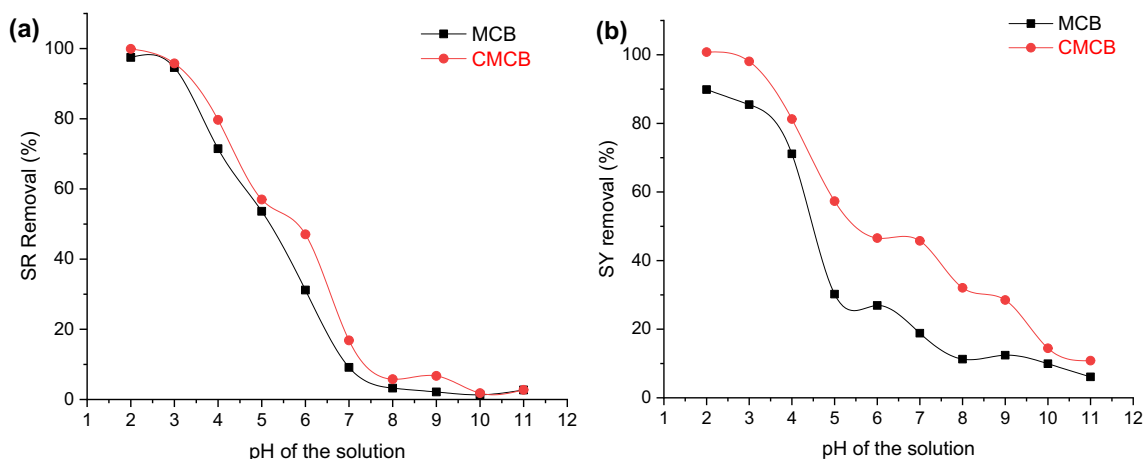


**Fig. 4** Effect of pH on **a** SR, **b** SY adsorption by MCB and CMCB (room temperature, 12 h, 180  $\text{r min}^{-1}$ , dye concentration: 50  $\text{mg L}^{-1}$ )



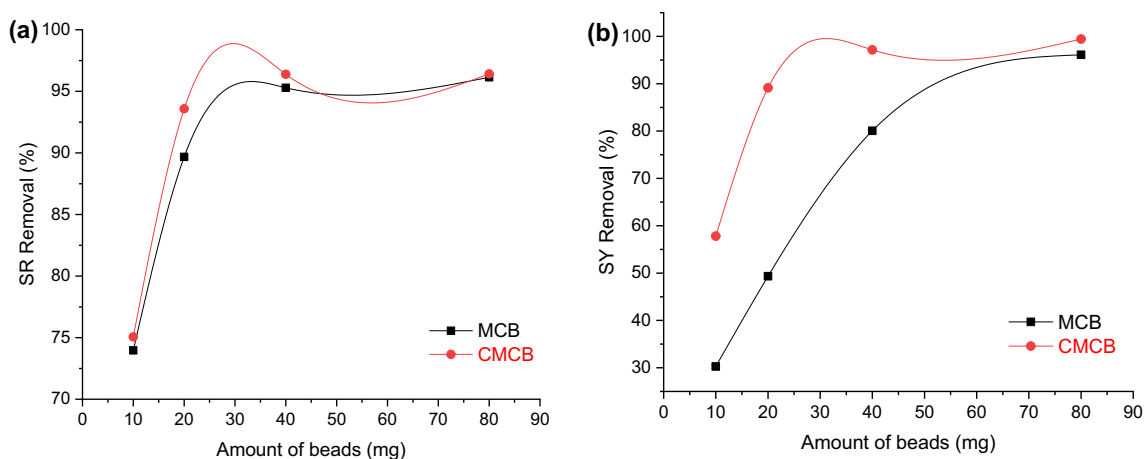


**Fig. 5** Effect of adsorbent dose on **a** SR, **b** SY adsorption by MCB and CMCB (room temperature, pH=2, 12 h, 180 r min<sup>-1</sup>, dye concentration: 50 mg L<sup>-1</sup>)

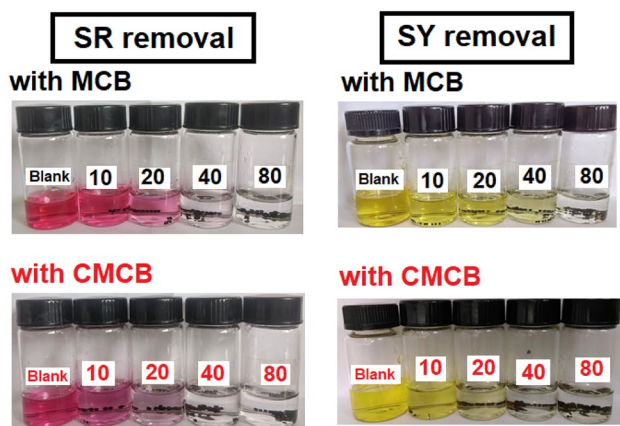


**Fig. 6** Experimental representation of the influence of the adsorbent dose on SR and SY removal. The experiments were carried out using 10–80 mg of beads, pH=2, room temperature, 180 r min<sup>-1</sup> and dye concentration 50 mg L<sup>-1</sup>. Blank: initial dye solution

Figure 5a, b show similar behavior in the adsorption of the two dyes: higher percentages of removal efficiency are obtained as the amount of beads increases. In SY removal, the adsorbent doses above 20 mg showed similar values using MCB (max. 96.14%) and CMCB (max. 96.42%). On the contrary, in SR removal, the doses above 20 mg showed similar percentage values for CMCB (max. 99.42%) but not for MCB (max. 96.10%). These results enable us to consider 20 mg as the optimal dosage.

Table S3 shows an improvement in the adsorption processes for coated MCB since the material, as demonstrated above, is more stable and displays an enhanced interaction with the azo dye.

### Effect of initial concentration

Initial dye concentration is a fundamental factor that helps to study the adsorption capacity of a material. The experiments were conducted with dye concentrations ranging from 20 to 600 mg L<sup>-1</sup>, at pH 2, a temperature of 25 °C, and a shaking speed of 180 r min<sup>-1</sup>.

Figure 7 shows an enhancement of the adsorption capacities as the initial dye concentration increases. The latter occurs because a higher concentration allows more dye molecules to interact with the beads' amino groups. According to Fig. 7a, maximum adsorption capacities ( $Q_{max}$ ) were 88.13 (MCB) and 192.03 (CMCB) mg g<sup>-1</sup> for SR, showing an increment of 54.1% when we used CMCB as an adsorbent. Figure 7b shows that the  $Q_{max}$  values were 57.4 (MCB) and 70.1 (CMCB) mg g<sup>-1</sup>. Herein, the increase in  $Q_{max}$  is not significant and may be produced by the presence of amino groups in SY structure (Fig. 8) that can also be protonated under acidic conditions, generating certain repulsions with the dye molecules and decreasing the  $Q_{max}$  values.

There is a higher degree of SR adsorption than SY because of their different structures. As shown in Fig. 8, SR has one more sulfonic group than SY, enhancing its interaction with the adsorbents.

The comparison of  $Q_{max}$  values obtained by MCB, CMCB, and other adsorbents (Kalkan et al. 2012; Kamranifar et al. 2018; Amin et al. 2020) is shown in Table 3. It is noticed that the adsorption capacity of CMCB is comparable with the results obtained for different materials.

### Effect of shaking speed

The effect of shaking speed in SR and SY adsorption was also investigated. Experimental results with speed values between 50 and 200 r min<sup>-1</sup> at pH 2, room temperature,



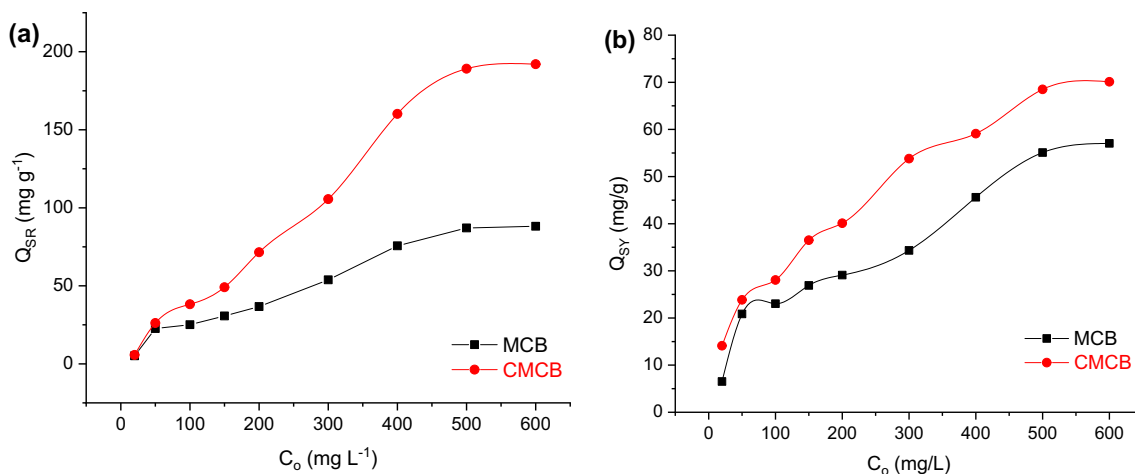


**Fig. 7** Effect of initial concentration on **a** SR, **b** SY adsorption by MCB and CMCB (room temperature,  $\text{pH}=2$ , 20 mg of beads, 12 h,  $180 \text{ r min}^{-1}$ )

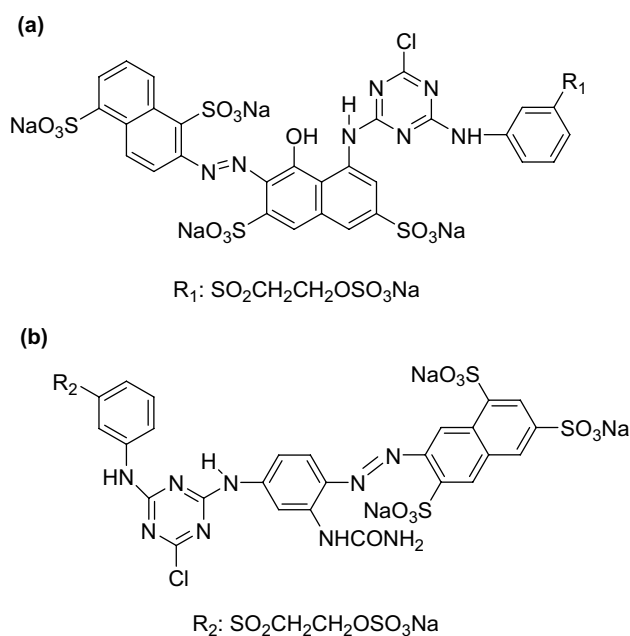


**Fig. 8** Structure of textile dyes. **a** Synozol Red HF-2GR, **b** Synozol Yellow HF-2BN

and  $50 \text{ mg L}^{-1}$  dye are shown in Fig. 9. According to Fig. 9a, b, greater dye removal percentages are obtained when the speed increases. This behavior relies on the presence of multiple magnetic domains in the two types of magnetic beads that enable better interaction with the textile dyes.

Figure 9 demonstrates the efficiency of removing azo dyes when CMCB is used as an adsorbent (Table S4). Besides, the shaking speed above  $180 \text{ r min}^{-1}$  shows similar percentage values compared to the results obtained at  $200 \text{ r min}^{-1}$ .

Based on this sense,  $180 \text{ r min}^{-1}$  was selected as the optimal value for speed.

### Adsorption isotherms

An adsorption isotherm is essential because it describes the interaction mechanism between the adsorbate and the adsorbent under equilibrium conditions. In this regard, the amount of solute adsorbed (per unit weight of adsorbent) is correlated with the concentration of the adsorbate in bulk solution (Sun et al. 2016).

Langmuir (Fig. S4) and Freundlich (Fig. 10) adsorption isotherm models were applied to fit the experimental data. All the isotherm parameters are listed in Table 4. The experimental results demonstrated that the Freundlich isotherm best represents the adsorption of SR and SY. In all cases, the correlation coefficients ( $R^2$ ) of the Freundlich model are more remarkable than the Langmuir model indicating that the adsorption process on the surface of the two adsorbents involves a multilayer sorption produced by the heterogeneous distribution of cross-linked chitosan.

The adsorption of the azo dyes displayed values of the parameter “ $n$ ” of 1.29 (SR–MCB), 1.02 (SR–CMCB), 1.78 (SY–MCB), and 2.10 (SY–CMCB). Since all the obtained values are greater than 1, this could indicate that the adsorption process is mainly governed by physisorption (Meroufel et al. 2013). The latter supports the electrostatic interactions between protonated amino groups of the adsorbents and sulfonic groups (SR, SY).

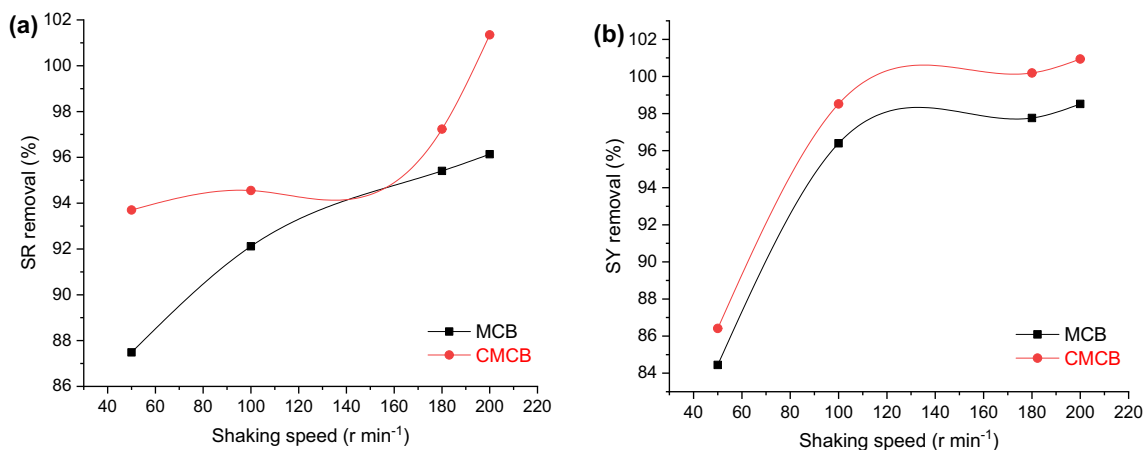
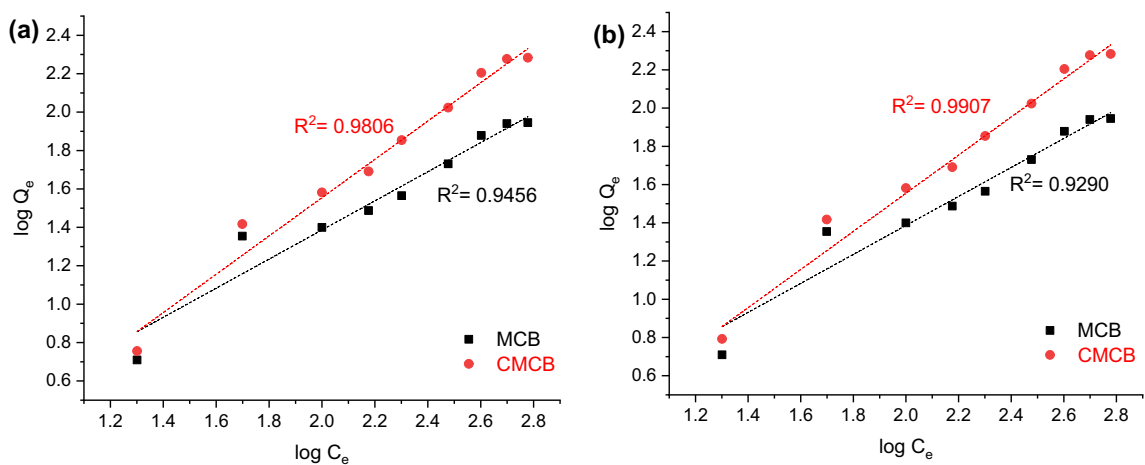
### Adsorption kinetics

The effect of contact time on dyes adsorption by MCB and CMCB was determined. Kinetic experiments were carried



**Table 3** Comparison of  $Q_{\max}$  of different adsorbents for SR and SY removal

SR dye			SY dye		
Material	$Q_{\max}$ (mg g <sup>-1</sup> )	References	Material	$Q_{\max}$ (mg g <sup>-1</sup> )	References
MCB	88.13	This work	MCB	57.4	This work
CMCB	192.03	This work	CMCB	70.1	This work
Cross-linked chitosan/oxalic acid hydrogel	110.7	(Pérez-Calderón et al. 2020)	Chitosan-coated magnetite nanoparticles	47.62	(Kalkan et al. 2012)
Chitosan coacervated particles	82.1	(Pérez-Calderón et al. 2018)	Extracted biochar	57.84	(Amin et al. 2020)
Barberry stem	27.2	(Kamranifar et al. 2018)			

**Fig. 9** Effect of shaking speed on **a** SR, **b** SY adsorption by MCB and CMCB (room temperature, pH=2, 20 mg of beads, 12 h, 180 r min<sup>-1</sup>, dye concentration: 50 mg L<sup>-1</sup>)**Fig. 10** Freundlich isotherms for SR (a) and SY (b) adsorption

out between 0 and 300–350 min, at pH 2, temperature of 25 °C, dye concentration of 50 mg L<sup>-1</sup>, 300 mL of solution, and 600 mg of beads.

CMCB displays high adsorption values than MCB in the two dyes adsorption processes (Fig. S5). As shown in Fig. S5a, SR adsorption reached equilibrium within 160–220 min

**Table 4** Adsorption isotherm parameters for SR and SY adsorption to MCB and CMCB

Isotherm model	SR–MCB	SR–CMCB	SY–MCB	SY–CMCB
Langmuir model				
$Q_m$ (mg g <sup>-1</sup> )	181.82	3333.3	75.18	88.49
$K_L$	$1.59 \times 10^{-3}$	$1.12 \times 10^{-4}$	$4.21 \times 10^{-3}$	$5.63 \times 10^{-3}$
$R^2$	0.7094	0.0319	0.8957	0.9555
Freundlich model				
$n$	1.29	1.02	1.78	2.10
$K_f$	0.681	0.401	1.58	3.416
$R^2$	0.9456	0.9806	0.9290	0.9907

**Table 5** Kinetic parameters for the removal of SR and SY by MCB and CMCB

Isotherm model	SR–MCB	SR–CMCB	SY–MCB	SY–CMCB
Lagergen model				
$Q_e$	16.21	19.29	14.46	16.67
$K_1$ (min <sup>-1</sup> )	0.019	0.021	$1.15 \times 10^{-3}$	$9.21 \times 10^{-4}$
$R^2$	0.8247	0.9850	0.6444	0.5116
Ho model				
$K_2$ (g mg <sup>-1</sup> min <sup>-1</sup> )	0.0059	0.0018	0.0167	0.0298
$R^2$	0.9999	0.9996	0.9989	0.9998
$Q_e$	25.31	28.82	9.64	9.82

for MCB and 140–160 min for CMCB. On the other hand, Fig. S5b shows that SY adsorption reached equilibrium within 80–150 min for MCB and 60–120 min for CMCB.

The experimental data were fitted to pseudo-first-order (Lagergren) and pseudo-second-order (Ho) kinetic models. Table 5 shows that the correlation coefficients ( $R^2$ ) for the

**Table 6** Desorption results

Cycle	SR–MCB (%)	SR–CMCB (%)	SR–NMCB (%)	SY–NMCB (%)
1	97.4	96.3	99.8	100.7
2	95.5	93.5	97.5	97.1

pseudo-second-order (Fig. 11) were higher than those of the pseudo-first-order model. These adjustments suggest that the adsorption process is governed by chemisorption, which involves an ion exchange or specific interaction with surface functional groups (Sun et al. 2016; Muedas-Taipe et al. 2020).

### Desorption and reusability experiment

The reusability of the adsorbents is critical in their potential application for SR and SY removal in real samples. This research used a 2 M NaOH solution (pH 10) to remove the dye from the surface of the adsorbent. Under basic conditions, the amino groups of the adsorbents are deprotonated, and the electrostatic interactions with the dyes are weakened. However, the pH of the desorption solution should be greater than eight since the chitosan can still sorb dye molecules at pH values of 6–8 (Kyzas and Lazaridis 2009).

Table 6 shows the adsorption of SR and SY by MCB and CMCB in two cycles of use. As can be seen, there is a decrease in the percentages of dye removal; however, this is not great enough to avoid performing more adsorption cycles. These experimental results demonstrate that our magnetic materials could be potentially reusable.

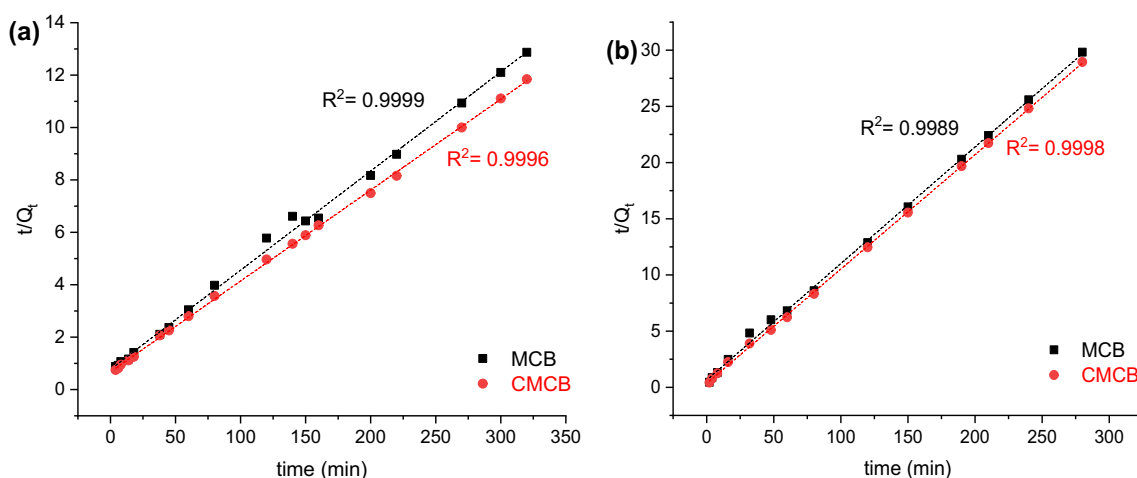


**Fig. 11** Pseudo-second-order model for SR (a) and SY (b) adsorption

## Adsorption of dye mixtures

The efficiency of adsorbents in some dye mixtures was also evaluated. The conditions of these experiments were: pH 2, temperature 25 °C, 20 mg of beads, shaking speed of 180 r min<sup>-1</sup>, and contact time of 3 h.

Experimental results are depicted in Fig. 12 and Table S6. A concentration ratio gives the proportion of dyes in each mixture. When the mixture is of a 1:1 concentration ratio, higher percentages of SR removal are obtained for the two adsorbents. This trend can be related to our previous hypothesis that implies the possible protonation of the amino group (of amide) present in the SY structure, decreasing the electrostatic interactions and affecting the efficiency of the adsorbents.

For the mixture of 1:2 concentration ratio (higher SY content), the percentages of SY removal were slightly more significant than those corresponding to SR because there are more molecules of SY azo dye. The mixture of a 2:1 concentration ratio (higher SR content) showed similar behavior with greater percentages of SR removal.

According to Table S6, the obtained values for mixtures are comparable to the ones obtained for the adsorption of the dyes separately, supporting the strong affinity of the adsorbents with the dyes. These results provide a basis for the adsorption of mixtures that include more dyes.

## Experimental design

The Box–Behnken designs demonstrated that our synthesized beads could remove a high concentration of azo dyes (100 mg L<sup>-1</sup>) and analyze the effect of using a significant adsorbent dose (80 mg). The properties of the designs were

checked to ensure that the standard error was lesser than one to guarantee reasonable confidence in the prediction. Table S7 shows the factor combinations and responses obtained for two dyes (SR and SY).

## Response surface methodology

Two modified Box–Behnken designs were built, one for each type of bead. Each design consisted of 17 experiments, corresponding to combinations of the selected independent variables with the following values: pH: 2.0, 3.0, and 4.0, the concentration of dye: 20.0, 50.0, and 100.0 mg L<sup>-1</sup>, and adsorbent dose 20.0, 40.0, and 80.0 mg. In each case, the percentages of dye removal were evaluated for all 17 experiments, and the corresponding polynomial models were fitted by least squares, according to Eq. (6). The model coefficients were computed by backward multiple regression ( $p < 0.10$ ) and validated by ANOVA. The best models adjusted a couple of responses corresponding to each design (Table 7).

As can be appreciated in Table 7, the four responses can be fitted with significant models ( $p < 0.05$ ), indicating a good relationship between the factors under study and responses. The first three models require quadratic polynomials, while the last is well-adjusted with a linear model. Interestingly, the lack of fit test was significant in all four cases, with  $p$ -values under 0.05. A visual inspection of the data presented in Table S7 reveals that this significant LOF is not caused by a poor fitting but by the high precision obtained by measuring the replicated standard experiments (numbers 13–17). This high repeatability results in a low value of pure error, generating large  $F$ -values and, consequently, low  $p$ -values. Thus, this statistical should not be considered.

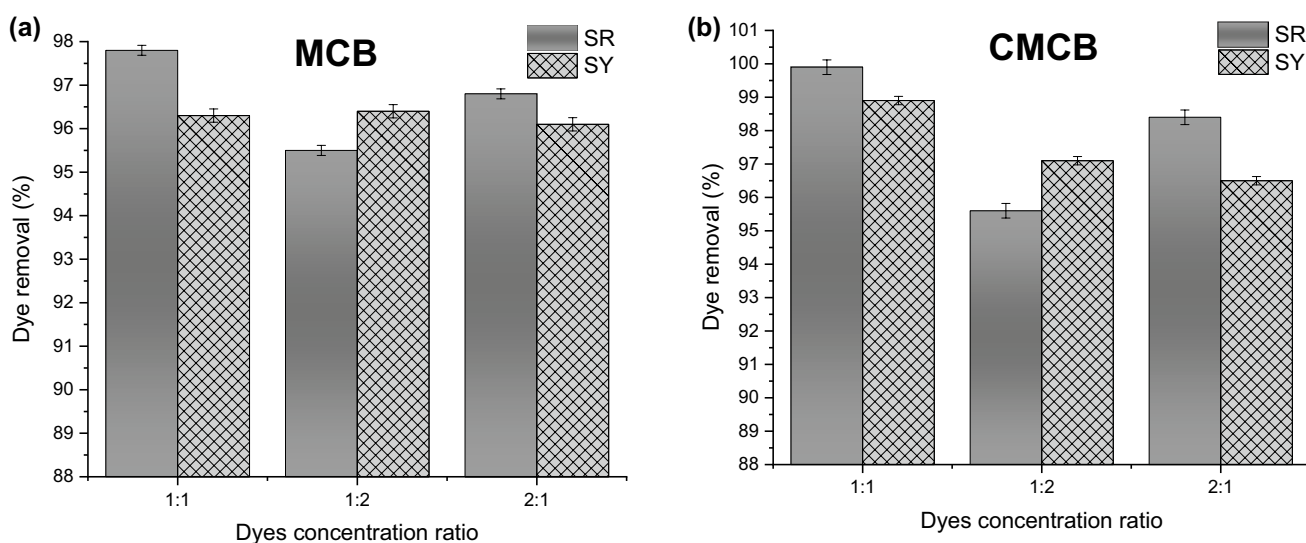


**Fig. 12** Adsorption of dye mixtures in different concentration ratios (room temperature, pH=2, 180 rpm). **a** MCB, **b** CMCB



**Table 7** Model fittings for the responses obtained from the experimental designs

Response	Model	Significant Terms <sup>a</sup>	ANOVA <i>p</i> -value <sup>b</sup>		<i>R</i> <sup>2</sup> <sub>adj</sub>
			Model	Lack of fit <sup>c</sup>	
SR–MCB	Quadratic	A (<0.0001) B (<0.0001) C (0.010) AB (0.092) A <sup>2</sup> (0.069) B <sup>2</sup> (0.002) C <sup>2</sup> (0.012)	<0.0001	0.003	0.9922
SY–MCB	Quadratic	A (0.023) B (<0.0001) C (0.0004) A <sup>2</sup> (<0.0001) B <sup>2</sup> (<0.0001) C <sup>2</sup> (0.0001)	<0.0001	<0.0001	0.9820
SR–CMCB	Quadratic	A (<0.0001) B (<0.0001) C (0.030) A <sup>2</sup> (<0.0001) B <sup>2</sup> (<0.0001)	<0.0001	<0.0001	0.9731
SY–CMCB	Linear	A (0.002) B (<0.0001) C (0.025)	<0.0001	<0.0001	0.9665

<sup>a</sup>A: pH, B: concentration of dye, and C: adsorbent dose. The numbers between parentheses correspond to *p*-values

<sup>b</sup>*p*-values less than 0.05 indicate significance

<sup>c</sup>Lack of fit should be non-significant, but there is high precision in the repetitions producing a low pure error (see in the text) and consequently a *p* > 0.05 for this test in all the cases

### Multiresponse optimization

The two sets of responses were simultaneously optimized using the desirability function, as indicated in Eq. (7). The criterion followed for optimizing the individual responses was their maximization. Lower and upper limits were: SR–MCB: 49.3–107.8%, SY–MCB: 30.3–96.5%, SR–CMCB: 78.4–110.2%, and SY–CMCB: 48.2–99.4%. The importance assigned to each response was the same. The optimal experimental conditions obtained for the mentioned optimization criterion corresponded to the following maxima in the desirability functions: *D*<sub>1</sub> = 0.950 and *D*<sub>1</sub> = 0.952. The first optimum (SR–MCB = 107.7% and SY–MCB = 96.5%) was reached under the following factor combinations: pH = 2.0, concentration = 20.0 mg L<sup>-1</sup>, and dose = 70.0 mg. The second optimum (SR–CMCB = 109.2% and SY–CMCB = 101.9%) was reached under the following factor combinations: pH = 2.0, concentration = 20.0 mg L<sup>-1</sup>, and dose = 80.0 mg.

According to the later observations, it can be recommended the second system for applying CMCB in a textile effluent to clean up this water.

Figure 13 shows the response surface and the contour plot for the desirability (*D*) corresponding to factors pH versus concentration for the second type of beads, maintaining the third factor at its optimal value (dose = 80.0 mg).

Finally, an experimental check was performed, obtaining the percentage of recovery under the optimal conditions predicted by the modeling. For design number 1, the experiment performed at pH = 2.0, concentration = 20.0 mg L<sup>-1</sup>, and dose = 70.0 mg rendered 106.9 and 96.1% (predicted values were 107.7 and 96.5%, respectively). For design number 2, the experiment was carried out at pH = 2.0, concentration = 20.0 mg L<sup>-1</sup> and dose = 80.0 mg rendered 108.4 and 101.1% (predicted values were 109.2 and 101.9%, respectively). It can be concluded that the matching among predicted and experimental values is indicative of the good quality of the analysis performed.



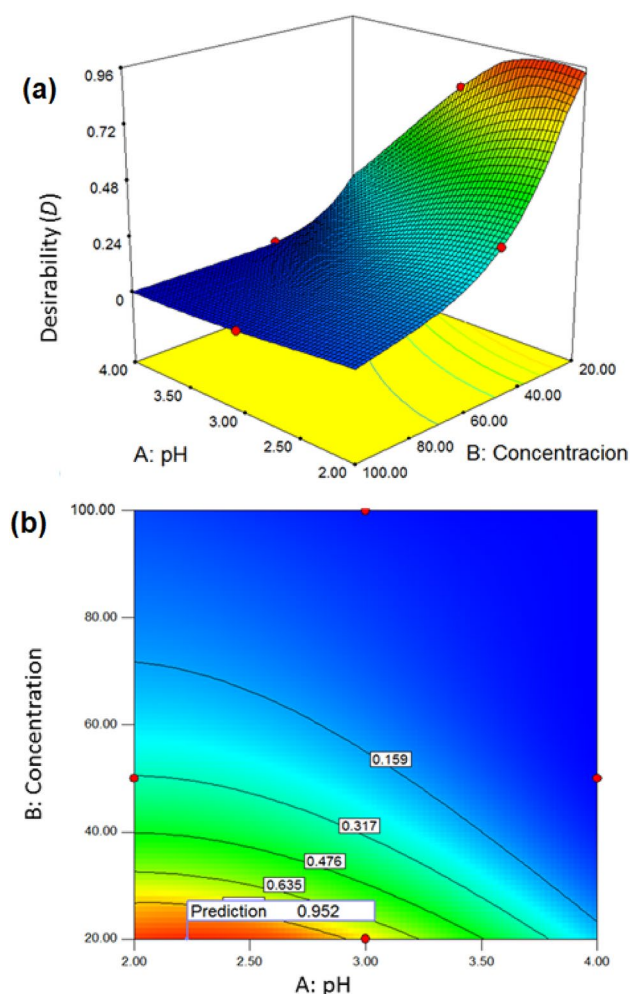


**Fig. 13** Global desirability function for CMCB. **a** Response surface, **b** contour plot. Both corresponding to factors pH versus concentration maintain the third factor at its optimal value (adsorbent dose = 80 mg)

## Conclusion

In conclusion, uncoated and coated with TEOS magnetic chitosan beads were successfully synthesized and characterized by FT-IR spectroscopy, SEM–EDX, and VSM. This series of analyses demonstrated that both materials maintain their morphologies and show magnetic responsive nature after an adsorption process supporting their potential reusability.

It was determined that the optimal pH was 2.0 because, under this condition, the amino groups of chitosan are protonated and interact well with the sulfonic ( $\text{SO}_3^-$ ) groups of the textile dyes. The maximum adsorption capacities for SR dye were 88.12 (MCB) and 192.02 (CMCB)  $\text{mg g}^{-1}$ , and for SY dye, the values were 57.03 (MCB) and 70.50 (CMCB)  $\text{mg g}^{-1}$ . CMCB showed higher adsorption capacity than MCB since the TEOS coating protects the

magnetic core from possible degradations, increasing the material's efficiency.

Adsorption equilibrium results fitted with the Freundlich isotherm model. The  $n$  values obtained from this model allowed us to verify the electrostatic interactions between the dye and the adsorbents. CMCB showed faster adsorption equilibrium times than uncoated MCB and other reported adsorbents for both dyes. Adsorption kinetic results were well suited for the pseudo-second-kinetic-order model indicating that the processes were governed by chemisorption.

A test involving the adsorption of a 1:1 dye mixture demonstrated the preference for the adsorbents to SR dye over SY dye.

Desorption experiments demonstrated the effective regeneration of the magnetic composites in continuous adsorption processes and its potential use in textile wastewater treatment.

The modeling of the data gathered by implementing a Box–Benken design furnished coefficients ( $R^2$  values) greater than 0.9, indicating a good correlation between the studied factors and responses. In addition, the implementation of a multiresponse optimization achieved a good correlation with the experimental data showing that the optimal conditions were pH 2, 20.0  $\text{mg L}^{-1}$  dye concentration, and 70–80 mg of adsorbent dose. These results provide the basis for expanding the model to the simultaneous optimization of responses involving many dyes to mimic the conditions of real textile wastewater samples accurately.

**Supplementary Information** The online version contains supplementary material available at <https://doi.org/10.1007/s13762-023-04769-0>.

**Acknowledgements** The authors of this research would like to thank the collaboration of Ph. D. Jose Carlos Diaz Rosado and Ph.D. Abel Gutarra from the Physics Department of “Universidad Nacional de Ingeniería” (National University of Engineering) for the obtention of SEM-EDX and hysteresis curves, respectively. Furthermore, the authors thank to Ph. D. Pilar Taboada from the Chemistry Institute of Araquara (Sao Paulo) for the obtention of the X-ray diffractograms.

## Declaration

**Conflict of interest** All the authors declare no conflict of interest.

## References

- Adar E (2020) Optimization of triple dye mixture removal by oxidation with Fenton. *Int J Environ Sci Technol* 17:4431–4440. <https://doi.org/10.1007/s13762-020-02782-1>
- Amin M, Chetpattananondh P, Khan MN (2020) Ultrasound assisted adsorption of reactive dye-145 by biochars from marine *Chlorella* sp. extracted solid waste pyrolyzed at various temperatures. *J Environ Chem Eng* 8:104403. <https://doi.org/10.1016/j.jece.2020.104403>
- Ayub A, Raza ZA, Majeed MI et al (2020) Development of sustainable magnetic chitosan biosorbent beads for kinetic remediation

- of arsenic contaminated water. *Int J Biol Macromol* 163:603–617. <https://doi.org/10.1016/j.ijbiomac.2020.06.287>
- Benkhaya S, M'rabet S, El Harfi A (2020) A review on classifications, recent synthesis and applications of textile dyes. *Inorg Chem Commun* 115:107891. <https://doi.org/10.1016/j.inoche.2020.107891>
- Danalioğlu ST, Kerkez Kuyumcu Ö, Abdel Salam M, Bayazit ŞS (2018) Chitosan grafted SiO<sub>2</sub>-Fe<sub>3</sub>O<sub>4</sub> nanoparticles for removal of antibiotics from water. *Environ Sci Pollut Res* 25:36661–36670. <https://doi.org/10.1007/s11356-018-3573-y>
- Dayana I, Sembiring T, Tetuko AP et al (2019) The effect of tetraethyl orthosilicate (TEOS) additions as silica precursors on the magnetite nano-particles (Fe<sub>3</sub>O<sub>4</sub>) properties for the application of ferro-lubricant. *J Mol Liq* 294:111557. <https://doi.org/10.1016/j.molliq.2019.111557>
- de Assis Filho RB, Baptisttella AMS, de Araujo CMB et al (2021) Removal of textile dyes by benefited marine shells wastes: from circular economy to multi-phenomenological modeling. *J Environ Manage* 296:113222. <https://doi.org/10.1016/j.jenvman.2021.113222>
- de Mendonça ESDT, de Faria ACB, Dias SCL et al (2019) Effects of silica coating on the magnetic properties of magnetite nanoparticles. *Surf Interfaces* 14:34–43. <https://doi.org/10.1016/j.surfin.2018.11.005>
- de Silva CEF, da Gama BMV, da Gonçalves AHS et al (2020) Basic-dye adsorption in albedo residue: Effect of pH, contact time, temperature, dye concentration, biomass dosage, rotation and ionic strength. *J King Saud Univ Eng Sci* 32:351–359. <https://doi.org/10.1016/j.jksues.2019.04.006>
- Derringer G, Suich R (1980) Simultaneous optimization of several response variables. *J Qual Technol* 12:214–219. <https://doi.org/10.1080/00224065.1980.11980968>
- Dixit S, Garg S (2019) Development of an efficient recombinant bacterium and its application in the degradation of environmentally hazardous azo dyes. *Int J Environ Sci Technol* 16:7137–7146. <https://doi.org/10.1007/s13762-018-2054-7>
- Freundlich HMF (1906) Over the adsorption in solution. *J Phys Chem* 57:385–470. <https://doi.org/10.1515/zpch-1907-5723>
- Haddad M, Abid S, Hamdi M, Bouallagui H (2018) Reduction of adsorbed dyes content in the discharged sludge coming from an industrial textile wastewater treatment plant using aerobic activated sludge process. *J Environ Manage* 223:936–946. <https://doi.org/10.1016/j.jenvman.2018.07.009>
- Ho YS, McKay G (1998) Sorption of dye from aqueous solution by peat. *Chem Eng J* 70:115–124. [https://doi.org/10.1016/S0923-0467\(98\)00076-1](https://doi.org/10.1016/S0923-0467(98)00076-1)
- Kalkan NA, Aksoy S, Aksoy EA, Hasirci N (2012) Adsorption of reactive yellow 145 onto chitosan coated magnetite nanoparticles. *J Appl Polym Sci* 124:576–584. <https://doi.org/10.1002/app.34986>
- Kamari S, Shahbazi A (2021) High-performance nanofiltration membrane blended by Fe<sub>3</sub>O<sub>4</sub>@SiO<sub>2</sub>-CS bionanocomposite for efficient simultaneous rejection of salts/heavy metals ions/dyes with high permeability, retention increase and fouling decline. *Chem Eng J* 417:127930. <https://doi.org/10.1016/j.cej.2020.127930>
- Kamranifar M, Khodadadi M, Samiei V et al (2018) Comparison the removal of reactive red 195 dye using powder and ash of barberry stem as a low cost adsorbent from aqueous solutions: isotherm and kinetic study. *J Mol Liq* 255:572–577. <https://doi.org/10.1016/j.molliq.2018.01.188>
- Kyzas GZ, Lazaridis NK (2009) Reactive and basic dyes removal by sorption onto chitosan derivatives. *J Colloid Interface Sci* 331:32–39. <https://doi.org/10.1016/j.jcis.2008.11.003>
- Lagergren S (1898) About the theory of so-called adsorption of soluble substances. *Kungliga Svenska Vetenskapsakademiens Handl* 24:1–39
- Langmuir I (1918) The adsorption of gases on plane surfaces of glass, mica and platinum. *J Am Chem Soc* 40:1361–1403. <https://doi.org/10.1021/ja02242a004>
- Lellis B, Fávaro-Polonio CZ, Pamphile JA, Polonio JC (2019) Effects of textile dyes on health and the environment and bioremediation potential of living organisms. *Biotechnol Res Innov* 3:275–290. <https://doi.org/10.1016/j.biori.2019.09.001>
- Liu Z, Wang H, Li B et al (2012) Biocompatible magnetic cellulose-chitosan hybrid gel microspheres reconstituted from ionic liquids for enzyme immobilization. *J Mater Chem* 22:15085–15091. <https://doi.org/10.1039/C2JM33033D>
- Mahdavinia GR, Etemadi H, Soleymani F (2015) Magnetic/pH-responsive beads based on carbonylmethyl chitosan and κ-carrageenan and controlled drug release. *Carbohydr Polym* 128:112–121. <https://doi.org/10.1016/j.carbpol.2015.04.022>
- Meroufel B, Benali O, Mohamed B et al (2013) Adsorptive removal of anionic dye from aqueous solutions by Algerian kaolin: characteristics, isotherm, kinetic and thermodynamic studies. *J Mater Environ Sci* 4:482–491
- Moradlou O, Dehghanpour Farashah S, Masumian F, Banazadeh AZ (2016) Magnetite nanoplates decorated on anodized aluminum oxide nanofibers as a novel adsorbent for efficient removal of As(III). *Int J Environ Sci Technol* 13:1149–1158. <https://doi.org/10.1007/s13762-016-0941-3>
- Muedas-Taípe G, Maza Mejía IM, Santillan FA et al (2020) Removal of azo dyes in aqueous solutions using magnetized and chemically modified chitosan beads. *Mater Chem Phys* 256:123595. <https://doi.org/10.1016/j.matchemphys.2020.123595>
- Mustafa FS, Güran M, Gazi M (2020) Effective removal of dyes from aqueous solutions using a novel antibacterial polymeric adsorbent. *J Polym Res* 27:247. <https://doi.org/10.1007/s10965-020-02227-w>
- Myers RH, Montgomery DC, Anderson-Cook CM (2009) Response surface methodology: process and product optimization using designed experiments. John Wiley & Sons, New York
- Nnadozie EC, Ajibade PA (2020) Adsorption, kinetic and mechanistic studies of Pb(II) and Cr(VI) ions using APTES functionalized magnetic biochar. *Microporous Mesoporous Mater* 309:110573. <https://doi.org/10.1016/j.micromeso.2020.110573>
- Patil NN, Shukla SR (2015) Degradation of reactive yellow 145 dye by persulfate using microwave and conventional heating. *J Water Process Eng* 7:314–327. <https://doi.org/10.1016/j.jwpe.2015.08.003>
- Pérez-Calderón J, Santos MV, Zaritzky N (2018) Reactive RED 195 dye removal using chitosan coacervated particles as bio-sorbent: analysis of kinetics, equilibrium and adsorption mechanisms. *J Environ Chem Eng* 6:6749–6760. <https://doi.org/10.1016/j.jece.2018.10.039>
- Pérez-Calderón J, Santos MV, Zaritzky N (2020) Synthesis, characterization and application of cross-linked chitosan/oxalic acid hydrogels to improve azo dye (reactive red 195) adsorption. *React Funct Polym* 155:104699. <https://doi.org/10.1016/j.reactfunctpolym.2020.104699>
- Radoń A, Łoński S, Kądziołka-Gaweł M et al (2020) Influence of magnetite nanoparticles surface dissolution, stabilization and functionalization by malonic acid on the catalytic activity, magnetic and electrical properties. *Colloids Surf Physicochem Eng Asp* 607:125446. <https://doi.org/10.1016/j.colsurfa.2020.125446>
- Revathi M, Kavitha B, Vedhi C, Senthil Kumar N (2019) Electrochemical detection and quantification of Reactive Red 195 dyes on graphene modified glassy carbon electrode. *J Environ Sci Health Part C Environ Carcinog Ecotoxicol Rev* 37:42–54. <https://doi.org/10.1080/10590501.2019.1555331>
- Roh H, Kim Y, Kim YK et al (2019) Amino-functionalized magnetic chitosan beads to enhance immobilization of potassium copper hexacyanoferrate for selective Cs<sup>+</sup> removal and facile recovery. *RSC Adv* 9:1106–1114. <https://doi.org/10.1039/C8RA09386E>



- Samchetsabam G, Hussan A, Gon Choudhury T et al (2017) Impact of textile dyes waste on aquatic environments and its treatment. *Environ Ecol* 35(3C):2349–2353
- Santillán F, Rueda JC (2020) Removal of methylene blue by hydrogels based on N, N-Dimethylacrylamide and 2-Oxazoline macromonomer. *J Polym Res* 27:263. <https://doi.org/10.1007/s10965-020-02239-6>
- Singh AL, Chaudhary S, Kumar S et al (2022) Biodegradation of reactive yellow-145 azo dye using bacterial consortium: a deterministic analysis based on degradable metabolite, phytotoxicity and genotoxicity study. *Chemosphere* 300:134504. <https://doi.org/10.1016/j.chemosphere.2022.134504>
- Sun X, Li Q, Yang L, Liu H (2016) Chemically modified magnetic chitosan microspheres for Cr(VI) removal from acidic aqueous solution. *Particuology* 26:79–86. <https://doi.org/10.1016/j.partic.2015.11.003>
- Svetlichnyi VA, Shabalina AV, Lapin IN et al (2017) Characterization and magnetic properties study for magnetite nanoparticles obtained by pulsed laser ablation in water. *Appl Phys A* 123:763. <https://doi.org/10.1007/s00339-017-1390-7>
- Tabar Y, Toosi MR (2018) Adsorptive filtration of azo dyes by polysulfone membranes blended with polyaniline based MCM-48 mesopore prepared from rice husk. *Desalin Water Treat* 115:315–325
- Tian Y, Xu Z, Yang Y et al (2022) Magnetic solid phase extraction based on Fe<sub>3</sub>O<sub>4</sub>@SiO<sub>2</sub>@CTS nano adsorbent for the sensitive detection of trace polychlorinated biphenyls in environmental water samples. *Microchem J* 172:106947. <https://doi.org/10.1016/j.microc.2021.106947>
- Vera Candiotti L, De Zan MM, Cámara MS, Goicoechea HC (2014) Experimental design and multiple response optimization. Using the desirability function in analytical methods development. *Talanta* 124:123–138. <https://doi.org/10.1016/j.talanta.2014.01.034>
- Wang J, Chang F, Tang X et al (2020) Bacterial laccase of *Anoxybacillus ayderensis* SK3-4 from hot springs showing potential for industrial dye decolorization. *Ann Microbiol* 70:51. <https://doi.org/10.1186/s13213-020-01593-6>
- Xia Y, Wang G, Guo L et al (2020) Electrochemical oxidation of Acid Orange 7 azo dye using a PbO<sub>2</sub> electrode: parameter optimization, reaction mechanism and toxicity evaluation. *Chemosphere* 241:125010. <https://doi.org/10.1016/j.chemosphere.2019.125010>
- Yang W, Tang Q, Dong S et al (2016) Single-step synthesis of magnetic chitosan composites and application for chromate (Cr(VI)) removal. *J Cent South Univ* 23:317–323. <https://doi.org/10.1007/s11771-016-3076-2>
- Yue R, Chen Q, Li S et al (2018) One-step synthesis of 1,6-hexanediamine modified magnetic chitosan microspheres for fast and efficient removal of toxic hexavalent chromium. *Sci Rep* 8:11024. <https://doi.org/10.1038/s41598-018-29499-z>
- Zhang Q, Zhuang S, Wang J (2020) Biosorptive removal of cobalt(II) from aqueous solutions using magnetic cyanoethyl chitosan beads. *J Environ Chem Eng* 8:104531. <https://doi.org/10.1016/j.jece.2020.104531>

Springer Nature or its licensor (e.g. a society or other partner) holds exclusive rights to this article under a publishing agreement with the author(s) or other rightsholder(s); author self-archiving of the accepted manuscript version of this article is solely governed by the terms of such publishing agreement and applicable law.

